IFASD 2015
International Forum on Aeroelasticity and Structural Dynamics
June 28 — July 02, 2015 ▲ Saint Petersburg, Russia

FLIGHT MECHANICAL MODELING AND ANALYSIS OF MULTI-BODY AIRCRAFT

Alexander Köthe[1] and Robert Luckner[2]

[1]Research Assistant at the
Institut für Luft- und Raumfahrt, Technische Universität Berlin
Marchstraße 12, 10587 Berlin, Germany
alexander.koethe@ilr.tu-berlin.de

[2]Full Professor at the
Institut für Luft- und Raumfahrt, Technische Universität Berlin
Marchstraße 12, 10587 Berlin, Germany
robert.luckner@tu-berlin.de

Keywords. HALE-Aircraft, Multi-Body-Dynamics.

Abstract. High Altitude Long Endurance (HALE) aircraft contain a large aspect ratio and thus a low induced drag. Recent developments in this field are connected to highly flexible aircraft. Unfortunately, these aircraft have some inconveniences. At TU Berlin's department of Flight Mechanics, Flight Control and Aeroelasticity a new aircraft concept, especially for HALE aircraft, is investigated. It concentrates on the coupling of several individual rigid body aircraft to an aircraft formation with a high aspect ratio. This paper introduces the concept of such a multi-body aircraft and focuses on the flight mechanic modeling and analysis. The later use of it as a HALE aircraft is not part of this paper. From two up to ten rigid body aircraft are bounded in two different configurations to form a new aircraft system. A steady flight mechanic investigation is undertaken out to determine the flight performance in trimmed conditions. Based on the steady state, the dynamic flight mechanic investigation is carried out. The findings of both, of the steady and of dynamic investigation are used to define requirements for the aircraft design and the flight controller synthesis of a multi-body aircraft with the purpose as HALE aircraft.

1 INTRODUCTION

In recent years, High Altitude Long Endurance (HALE) aircraft have started to become an alternative for satellites, e.g. for communication and surveillance tasks, since they offer more flexibility in operation. Due to their lightweight construction, their high-aspect-ratio and the use of solar panels, they can be operated in the stratosphere for up to 336 hours (cf. QinetiQ Zephyr [8]). In contrast to satellites, HALE aircraft are not bounded to a specific trajectory. They can be operated in a specific region for a certain amount of time. After the mission's completion, they can be recovered, relocated and used in another region or for another mission. Although light weight structures and a long span can be used for HALE aircraft, there are some disadvantages: on one hand a large deformation of the wing leads to a geometrically nonlinear behavior in structural dynamics. This behavior must be represented with an accurate nonlinear aeroelastic framework. And on the other hand, they exhibit a direct impact into the flight dynamics

that led to catastrophic consequences during the Helios flight test program [1]. On the flight to the mission's altitude, the HALE aircraft passes the troposphere, in which most of the weather events (gust, turbulence) occur. Gusts may cause high aerodynamic loads leading to a high bending moment and thus influences the fatigue strength of the aircraft. Additionally, non uniform gust excitations of the highly flexible vehicle can occur that result into larger deformations than the uniform one [17].

At TU Berlin's department of Flight Mechanics, Flight Control and Aeroelasticity, a new concept for HALE aircraft is investigated. Several individual rigid-body aircraft are linked to build a single HALE aircraft. Advantages of such a multi-body aircraft are explained in the following. High-aspect-ratio can be accomplished without consideration of structural geometrical nonlinearities. Moreover, single bodies can be brought to the stratosphere with a helium balloon or fly on their own up to the mission's altitude ensuring low aerodynamic loads due to atmospheric disturbance in the troposphere. Lastly, the modularity of the multi-body aircraft permits individual exchange and return to ground of a single aircraft for repair without affecting significantly the flight mission.

1.1 Concept of multi-body aircraft

The concept of a multi-body aircraft is based on the idea that several individual aircraft are linked to build a HALE-aircraft in the mission's altitude. Each aircraft has a small wing-span, which means that it can be assumed as rigid. The individual is carried to the mission with a balloon or flying up on its own. This means that each aircraft has to be able to fly individually. Therefore, the aircraft requires an adequate wing to produce enough lift, a horizontal and vertical stabilizer for stability, control surfaces (ailerons, elevator and flaps) for lateral and vertical controllability and a flight control system. If two or more aircraft are at the mission's altitude, a specific flight control law is used to connect the individual aircraft to a HALE-aircraft. Two feasible connection configurations are examined.

The first configuration (abbreviated *Conf1DJ* in the following) permits a pitch motion between the individual aircraft. All other degrees of freedom between two coupled aircraft are restricted. As a result, each aircraft could feature an individual angle of attack. The additional degree of freedom allows a maneuver and gust load alleviation and thus a decrease of the bending moment of the aircraft formation. This enables a structural weight reduction. Nevertheless, it is worth mentionning that a bending moment of the formation further exists and in terms of a decrease of the wing stiffness, aeroelastic phenomenons, like flutter and divergence, can occur.

The second configuration (abbreviated *Conf2DJ* in the following) allows, due to the joint, a pitch and roll motion between the individual aircraft. All advantages of *Conf1DJ* are achieved, but, thanks to the joints, without transferring bending moments through the formation. As a consequence, a long span in connection with light weight structures can be used in aircraft design without a huge impact on aeroelastic phenomenons.

Beside the benefits regarding to the structural strain, a further advantage for the multi-body aircraft exist: In the case of any malfunction of the system or the payload of a single aircraft, the faulty aircraft releases the network and returns back to the base. For this

reason, the individual aircraft has to be able to operate as a stand-alone aircraft. In order to prove the advantages of this new aircraft concept regarding to flight performance and stability, a flight mechanic investigation is carried out by coupling two up to ten aircraft in both configurations.

1.2 Generic Unmanned Aerial Vehicle

In this paper, a qualitative study concerning the coupling of several aircraft shall be conducted. Therefore any suitable aircraft can be used. Due to the requirement that the single aircraft should operate as a stand-alone aircraft and unmanned, a generic UAV is used for the investigations. For this UAV, data regarding to the geometry, inertia and aerodynamic are available. This generic airplane is a propeller-powered airplane (a maximum thrust of 70 N) with a straight wing, a horizontal stabilizer and a double vertical tail. The wing span is about 4 m and a mass of 7.9 kg is considered for the analysis. Ailerons, flaps, rudder and an elevator are used as aircraft's flight control surfaces. The geometry of this generic aircraft is illustrated in figure 1. The centre of gravity is located in the middle of the wing chord and the associated minimum drag airspeed is 15 $\frac{\mathrm{m}}{\mathrm{s}}$.

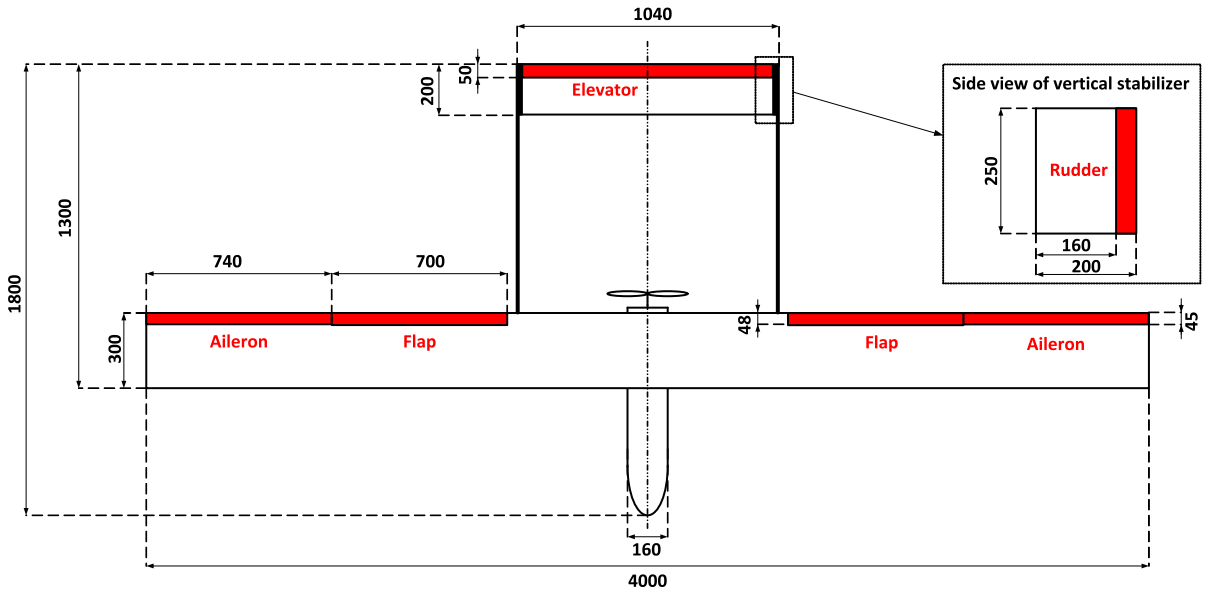

Figure 1: Schematic illustration of the generic UAV

2 FLIGHT MECHANIC MODEL OF THE MULTI-BODY AIRCRAFT

A flight mechanic model is necessary to investigate the steady and dynamic flight mechanic behavior of the multi-body aircraft and thus validate the postulated advantages of the new aircraft concept. There are a lot of possible approaches to estimate equations of motion. In the context of multi-body-dynamics, Kane's method is often used. Kane's method provides the benefits of both traditional approaches the Newton-Euler and Lagrange methods. Due to the use of generalized forces the necessity for examining interactive and constraint forces between bodies is eliminated. Since Kane's method does not use energy functions, differentiating of Lagrange function is no longer a difficulty. That is why the method is originally called Lagrange form of d'Alembert's principle [4]. Because of the advantages of this method, the equations of motion for the multi-body aircraft are assembled following Kane's formalism [5]. For this purpose, the multi-body-software

Autolev is used [9].

2.1 Equations of motion

The origin of the equations of motion using Kane's method is Kane's dynamical equation,

$$\underline{\tilde{F}}_r + \underline{\tilde{F}}_r^{\star} = 0 \quad (r = 1, \ldots, p)\,, \tag{1}$$

where $\underline{\tilde{F}}_r$ are the generalized active forces, $\underline{\tilde{F}}_r^{\star}$ are the generalized inertial forces and p is the number of degrees of freedom of the system in the reference frame. In equation 1, the denotation "generalized force" includes inertial and active forces as well as inertial and active moments (translation and rotation) [5]. The generalized inertial force is determined with

$$\underline{\tilde{F}}_r^{\star} = -\sum_{j=1}^{l} {}^{N}\underline{F}_k^{CG,j} \; \frac{\partial {}^{N}\underline{v}^{CG,j}}{\partial u_r} - \sum_{j=1}^{l} {}^{N}\underline{M}_k^{CG,j} \; \frac{\partial {}^{N}\underline{\omega}^{B,j}}{\partial u_r}, \tag{2}$$

where ${}^{N}\underline{v}^{CG,j}$ is the velocity of the centre of gravity of the jth body in the Newtonian frame, ${}^{N}\underline{\omega}^{B,j}$ the angular velocity of the body frame against the Newtonian frame of the jth body, u_r the generalized speeds and $\underline{F}_k$ and $\underline{M}_k$ are the mass force and mass torque of the jth body decomposed as

$${}^{N}\underline{F}_k^{CG} = m\left(\frac{d\,{}^{B}\underline{v}^{CG}}{dt} + {}^{N}\,\underline{\omega}^{B} \times {}^{B}\,\underline{v}^{CG}\right) \quad \text{and} \quad {}^{N}\underline{M}_k^{CG} = \underline{\underline{I}}^{N}\dot{\omega}^{B} + {}^{N}\,\omega^{B} \times \left(\underline{\underline{I}}\;{}^{N}\omega^{B}\right), \tag{3}$$

and l the number of rigid bodies in the system. The generalized active force is given by

$$\underline{\tilde{F}}_r = \sum_{j=1}^{l} {}^{N}\underline{F}_A^{CG,j} \; \frac{\partial {}^{N}\underline{v}^{CG,j}}{\partial u_r} + \sum_{j=1}^{l} {}^{N}\underline{M}_A^{CG,j} \; \frac{\partial {}^{N}\underline{\omega}^{B,j}}{\partial u_r}, \tag{4}$$

where $\underline{F}_A$ and $\underline{M}_A$ are the active forces and moments acting at or around the center of gravity. Both, velocities and angular velocities in equations 2 and 4 are based on generalized speeds $u_r\,(r = 1, \ldots, p)$ that are derived from the generalized coordinates $q_s\,(r = 1, \ldots, n)$, where n is the number of generalized coordinates and p the number of generalized speeds, with

$$u_r = \sum_{s=1}^{n} Y_{rs}\; \dot{q}_s + Z_r \quad (r = 1, \ldots, p) \tag{5}$$

where Y_{rs} and Z_r are functions of the generalized coordinates and time. Equation 5 is called kinematical differential equation [5]. The generalized coordinates uniquely describe the state of the configuration. For a multibody configuration composed of i rigid bodies with six degrees of freedom, the number of generalized coordinates is determined with

$$n = 6 \times i - M, \tag{6}$$

where M is the number of holonomic constraint equations. Nonholonomic constraint equations can be express as m relationship

$$u_r = \sum_{s=1}^{p} A_{rs}\; u_s + B_r \quad \text{with} \quad p = n - m \quad (r = p+1, \ldots, n) \tag{7}$$

where A_{rs} and B_r are functions of the generalized coordinates and time [5]. It should be noted that other kinds of nonholonomic constraints can exist in multi-body-systems (e.g. inequalities, such as restrictions on a specific motion area). In case of using equation 7, holonomic constraint equations can be formed into nonholonomic constraint equations, but not necessarily vice versa.

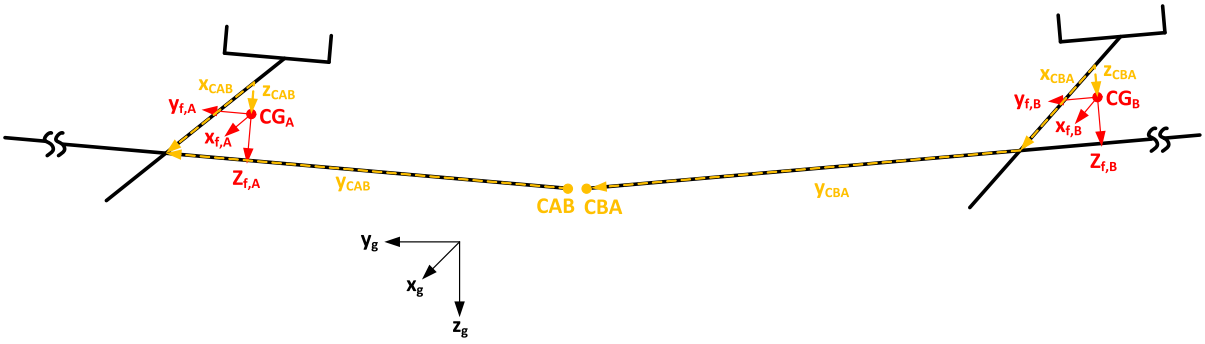

Figure 2: Example of two coupled aircraft for assembling the equations of motion

Those equations are sufficient to set up the equations of motion for the multi-body aircraft. The procedure for Kane's formalism is illustrated by considering the example of figure 2. In this case, two single aircraft are coupled to a new aircraft formation. Every single aircraft represents a rigid body with a body fixed reference frame. As a consequence, the position (three Cartesian coordinates) and the orientation against the Newtonian frame (three Euler angles[1]) are used as generalized coordinates. This results in six generalized coordinates per aircraft and thus twelve generalized coordinates for the whole formation. With the help of equation 5, the generalized speeds are determined. In order to calculate the position, the body fixed velocities are selected as generalized speeds. This means that functions Y_{rs} are equal to one and all Z_r equal to zero. For defining the orientation, the angular velocities for each axis are chosen as generalized speeds. This leads, going back to equation 5, to a dependence of Y_{rs} functions on the Euler angles and to a disapearance of Z_r functions, which are again equal to zero. Now, using the twelve generalized speeds, the kinematic equations for equations 3 and 2 (mass force and torque) as well as for the active forces (equation 4) can be set up.

Depending on the joint's configuration, nonholonomic as well as holonomic constraints exist or not. The joint is assumed as ideal without friction, damping or spring forces. The equations of constrain are exemplary introduced for two coupled aircraft that are illustrated in figure 2. The point CAB is the connection point of aircraft A and CBA of aircraft B. In configuration *Conf1DJ*, the five nonholonomic constraint equations, as illustrated in the free body diagram in figure 3, are formed with the followings relations:

$$\begin{array}{ll} \left({}^N\underline{v}^{CAB} - {}^N\underline{v}^{CBA}\right)\vec{e}_{xg} = 0 & \left({}^N\underline{v}^{CAB} - {}^N\underline{v}^{CBA}\right)\vec{e}_{yg} = 0 \\ \left({}^N\underline{v}^{CBA} - {}^N\underline{v}^{CAB}\right)\vec{e}_{zg} = 0 & \left({}^N\underline{\omega}^{A} - {}^N\underline{\omega}^{B}\right)\vec{e}_{xg} = 0 \\ \left({}^N\underline{\omega}^{A} - {}^N\underline{\omega}^{B}\right)\vec{e}_{zg} = 0 & \end{array} . \tag{8}$$

The velocities of the connection points in the Newtonian frame regarding to figure 2 can

[1]Euler angles is the denotation in flight mechanics. In multi-body-dynamics the orientation angles are mentioned as Cardan angles.

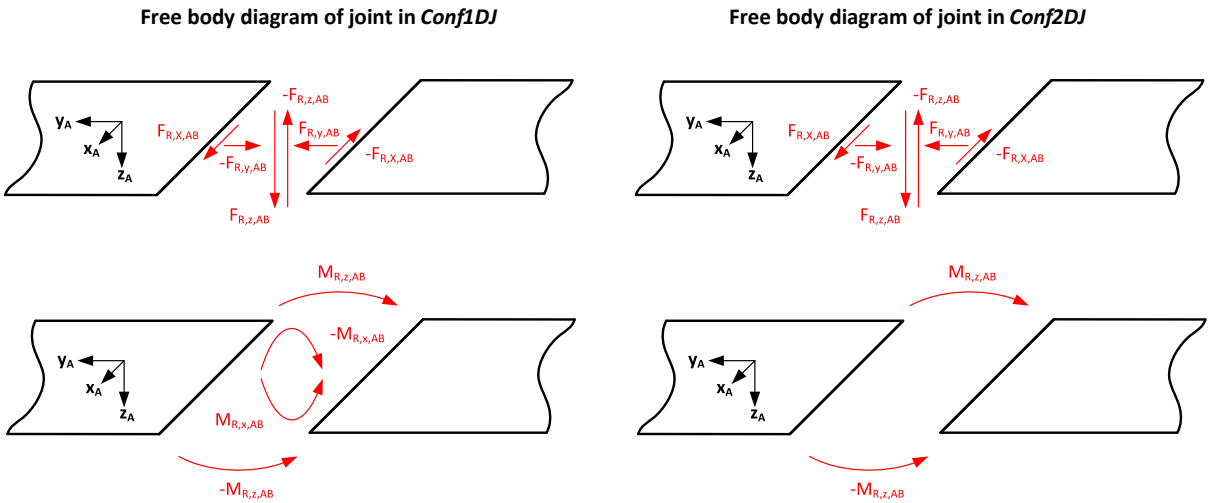

Figure 3: Free body diagramm of joint in the two considered configurations

be formulated

$$\begin{aligned} {}^N\underline{v}^{CAB} &= {}^N\underline{v}^{CG,A} + {}^N\underline{\omega}^{A} \times \underline{r}_{CAB} \quad \text{wherein} \quad \underline{r}_{CAB} = [x_{CAB}, \; -y_{CAB}, \; -z_{CAB}]^T \\ {}^N\underline{v}^{CBA} &= {}^N\underline{v}^{CG,B} + {}^N\underline{\omega}^{B} \times \underline{r}_{CBA} \quad \text{wherein} \quad \underline{r}_{CBA} = [x_{CAB}, \; y_{CAB}, \; -z_{CAB}]^T \end{aligned} \quad . \tag{9}$$

Those nonholonomic motion constrain can be expressed in holonomic constrains, if the generalized coordinates in equation 5 appear directly from the integration of the generalized speeds. This is the case, if the functions Y_{rs} and Z_r are independent of the generalized coordinates. Relating to the constrain equations of the velocity, this condition is fulfilled. Thus those nonholonomic constrain equations lead to holonomic constrain, which imply that the position between the connection points CAB and CBA is fixed. Since there is only one rotational degrees of freedom between the aircraft, the integrability condition is also fulfilled for the constrain equations of the angular velocity. Thus the system of two coupled aircraft for *Conf1DJ* contains $n = 7$ degrees of freedom and can be characterized by $p = 7$ generalized speeds and hence seven equations of motion. The procedure for the second configuration is similar. Now, the constraint equations are

$$\begin{aligned} \left({}^N\underline{v}^{CAB} - {}^N\underline{v}^{CBA}\right)\vec{e}_{xg} &= 0 \qquad \left({}^N\underline{v}^{CAB} - {}^N\underline{v}^{CBA}\right)\vec{e}_{yg} = 0 \\ \left({}^N\underline{v}^{CBA} - {}^N\underline{v}^{CAB}\right)\vec{e}_{zg} &= 0 \qquad \left({}^N\underline{\omega}^{A} - {}^N\underline{\omega}^{B}\right)\vec{e}_{zg} = 0 \end{aligned} \quad . \tag{10}$$

The $p = 3$ nonholonomic motion constrains for the body fixed velocities can be further expressed as $M = 3$ holonomic constrain equations. This is no longer applicable for the motion constrains of the rotation. Using the roll rate u_1, pitch rate u_2 and yaw rate u_3 as generalized speeds and the roll angle q_1, pitch angle q_2 and yaw angle q_3 as generalized coordinates, the following kinematic differential equations

$$\begin{bmatrix} \dot{q}_1 \\ \dot{q}_2 \\ \dot{q}_3 \end{bmatrix} = \begin{bmatrix} 1 & \sin(q_1)\tan(q_2) & \cos(q_1)\tan(q_2) \\ 0 & \cos(q_1) & -\sin(q_2) \\ 0 & \frac{\sin(q_1)}{\cos(q_2)} & \frac{\cos(q_1)}{\cos(q_2)} \end{bmatrix} \begin{bmatrix} u_1 \\ u_2 \\ u_3 \end{bmatrix} \tag{11}$$

are applied [10]. Even if u_3 equals to zero in equation 11 due to the nonholonomic motion constrains, the pitch and roll rate influence all other generalized speed. Thus there exist $p = 1$ nonholonomic constrain, but no holonomic contrains. As a result, the system of two coupled aircraft for the second configuration contains $n = 9$ degrees of freedom and can

be characterized by eight equations of motion and three additional kinematic differential equations. Those equations of motion are highly nonlinear due to the rotational degrees of freedom, but the existing nonlinearities can be described mathematically exact.

To handle the complexity of assembling the equations of motion, the multi-body-software Autolev, based on Kane's method, is used to generate a MATLAB code for the equations of motion. It has to be mentioned that the equations of motion can also be formulated with a reduced number of generalized coordinates. This means that it would not be possible to determine the reaction forces and moments from figure 3. That is the reason why this method was excluded despite of its effort in time calculation.

2.2 Active forces and moments

The active forces and moments that have to be considered for the equations of motion are: aerodynamic forces (in the aerodynamic reference frame) $\underline{R}_A$, thrust (in the body fixed reference frame) $\underline{T}$ and weight (in the Newtonian frame) $\underline{W}$ of each aircraft as well as aerodynamic moments (in the aerodynamic reference frame) $\underline{M}_A$ and thrust moments (in the body fixed reference frame) $\underline{M}_T$. For each single aircraft, it is assumed that the thrust acts at the center of gravity. This results in a zero thrust moment. Regarding to equation 4, the active force at the jth aircraft in the body fixed reference frame is determined with

$$ {}^{b}\underline{F}_A^{CG,j} = \underline{\underline{T}}_{b,a,j}\ \underline{R}_{A,j} + \underline{\underline{T}}_{b,n,j}\ \underline{W}_j + \underline{T}_j, \tag{12} $$

where $\underline{\underline{T}}_{b,a}$ is the transformation matrix from the aerodynamic reference frame (index a) to the body fixed reference frame (index b) and $\underline{\underline{T}}_{b,n}$ is the transformation matrix from the Newtonian reference frame (index n)[2] to the body fixed reference frame. The active moment of the jth aircraft in the body fixed reference frame for equation 4 is computed with

$$ {}^{b}\underline{M}_A^{CG,j} = \underline{\underline{T}}_{b,a,j}\ \underline{M}_{A,j} + \underbrace{\underline{M}_F}_{=0}. \tag{13} $$

2.2.1 Gravity and thrust

The gravity of the jth aircraft is defined in the Newtonian reference frame as

$$ \underline{W}_j = [0, \quad 0, \quad m_j\ g]^T \tag{14} $$

where m_j is the mass of the jth aircraft and g is the gravitational acceleration. The thrust of the jth aircraft is calculated with

$$ \underline{T}_j = [\eta_{F,j}\ F_{\mathrm{max,j}}, \quad 0, \quad 0]^T \tag{15} $$

where $\eta_{F,j}$ is the percentage used of the maximal thrust $F_{\mathrm{max,j}}$ for the jth aircraft. For the considered reference aircraft the maximal thrust is 70 N.

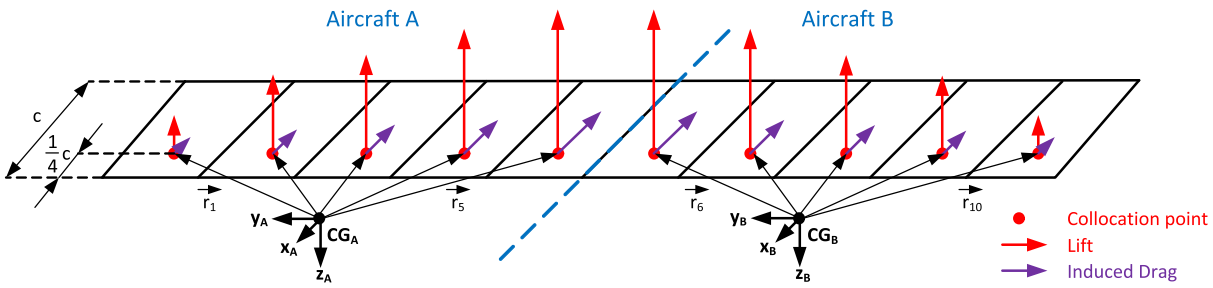

Figure 4: Illustration of aerodynamic forces at the wing by using the lifting-line method

2.2.2 Aerodynamic forces and moments

Aerodynamic forces and moments are generated by the wing, horizontal stabilizer and vertical stabilizer. The overall wing is built up by the wings of the single aircraft. As a consequence, a wing with a high aspect ratio is formed. The aerodynamic forces and moments are calculated with the lifting line method described in [6]. For this purpose, the wing is divided in a finite number of strips. On each strip, a collocation point is placed on the quarter chord and half span of the strip. With a horseshoe vortex, the circulation Γ_i and the induced downwind $w_{ind,i}$ at each collocation point is calculated depending on the angle of attack α_i, the sideslip angle β_i and the freestream velocity $V_{\infty,i}$. The lift of each strip L_i is obtained by using the Kutta-Joukowski theorem

$$L_i = \rho \; V_{\infty,i} \; \Gamma_i \; \Delta y \tag{16}$$

where ρ is the density and Δy the span of the strip. The induced drag at each collocation point $D_{ind,i}$ is computed with

$$D_{ind,i} = -\rho \; w_{ind,i} \; \Gamma_i \; \Delta y \tag{17}$$

as described in [6]. As mentioned, the results of lift and induced drag are influenced by the angle of attack, the sideslip angle and the freestream velocity, which, at the same time, are influenced by other parameters.

The yaw rate r_j of the jth aircraft affects the velocity V_i of the ith strip with

$$V_i = V_\infty - r_j \; y_i, \tag{18}$$

where y_i is the distance between the centre of gravity and the collocation point of the ith strip in spanwise direction. The angle of attack at the ith strip is influenced by the roll rate p_j and pitch rate q_j of the jth aircraft and, if the strip is flapped, by the flap deflection $\eta_{K,i}$ of the ith strip according to [13] with

$$\alpha_i = \alpha_{ref,j} + \frac{y_i}{V_i} p_j - \frac{x_i}{V_i} q_i - \frac{2}{\pi} \left(\sqrt{\lambda_{k,i} \left(1 - \lambda_{k,i}\right)} + \arcsin \sqrt{\lambda_{k,i}} \right) \eta_{K,i}, \tag{19}$$

where $\alpha_{ref,j}$ is the reference angle of attack of the jth aircraft, $\lambda_{k,i}$ the ratio between flap chord and the strip chord and x_i is the distance between the centre of gravity and the collocation point of the ith strip in nose direction.

[2] In Flight mechanics often mentioned as geodetic reference frame that is considered as inertial system.

Beside the induced drag, the zero drag $D_{0,j}$

$$D_{0,i} = \frac{\rho}{2}\, V_i^2\, S_i\, C_{D,0}, \tag{20}$$

where S_i is the area of the ith strip and $C_{D,0}$ the zero drag coefficient, and, if the strip is flapped, the drag due to flap deflection according to [12] with

$$D_{0,j} = \frac{\rho}{2}\, V_j^2\, S_j\, C_{D,\mathrm{Flap}} \quad \text{with} \quad C_{D,\mathrm{Flap}} = \lambda_{k,i} A \left(|\eta_{K,i}|\right)^B, \tag{21}$$

where $A = 0.0016$ and $B = 1.5$ [12] for a split flap, are considered for each strip. Furthermore, the side force of each strip is calculated depending on the side slip angle and the zero drag coefficient with

$$Y_i = -\frac{\rho}{2}\, V_j^2\, S_j\, C_{D,0}\, \sin\left(\beta_i\right), \tag{22}$$

where β_i is the side slip angle of each strip. If lift, drag and side force are calculated for each strip, the resulting aerodynamic forces $\underline{R}_{A,W}$ for the whole wing can be computed. Therefore, the forces are assigned to an aircraft depending on the collocation point position. The resulting aerodynamic moments for each aircraft are determined with the cross product of the distance between the center of gravity and the collocation point $\underline{r}_i$, as well as the force vector. Regarding to the example of figure 4, the aerodynamic forces and moments for each aircraft are

$$\begin{aligned} \underline{R}_{A,W,A} &= \sum_{i=1}^{5} \begin{bmatrix} -D_i \\ Y_i \\ -L_i \end{bmatrix} & \underline{R}_{A,W,B} &= \sum_{i=6}^{10} \begin{bmatrix} -D_i \\ Y_i \\ -L_i \end{bmatrix} \\ \underline{M}_{A,W,A} &= \sum_{i=1}^{5} \left(\underline{r}_i \times \begin{bmatrix} -D_i \\ Y_i \\ -L_i \end{bmatrix} \right) & \underline{M}_{A,W,B} &= \sum_{i=6}^{10} \left(\underline{r}_i \times \begin{bmatrix} -D_i \\ Y_i \\ -L_i \end{bmatrix} \right) \end{aligned} . \tag{23}$$

In addition to the forces from equation 23, the aerodynamic forces acting at the jth tail

$$\begin{bmatrix} -D_{T,j} \\ Q_{T,j} \\ -L_{T,j} \end{bmatrix} = \frac{\rho}{2} V_j^2 \begin{bmatrix} S_{HS,j} \left(C_{D,\eta}\, \eta_j + \frac{\left(C_{L,\alpha,T}\ \alpha_{tail,j} + C_{L,\eta,T}\ \eta_j\right)^2}{\pi\ \Lambda_H\ e} \right) \\ S_{VS,j}\ \left(C_{Y,\beta,T}\ \beta_{tail,j} + C_{Y,\zeta,T}\ \zeta_j\right) \\ S_{HS,j}\ \left(C_{L,\alpha,T}\ \alpha_{tail,j} + C_{L,\eta,T}\ \eta_j\right) \end{bmatrix}, \tag{24}$$

where S_{HS} is the area of the horizontal stabilizer and S_{VS} the area of the vertical stabilizer, η_j the elevator and ζ_j the ruder deflection, Λ_H the aspect ratio and e the Oswald factor of the horizontal stabilzer, as well as the aerodynamic moments

$$\underline{M}_{A,T,j} = r_{T,j} \times \begin{bmatrix} -D_{T,j} \\ Q_{T,j} \\ -L_{T,j} \end{bmatrix}, \tag{25}$$

where $r_{T,j}$ is the position vector from the centre of gravity to the neutral points of the horizontal and vertical stabilizer, have to be considered. The angle of attack $\alpha_{tail,j}$ at the jth stabilizer is influenced by the downwind $w_{ind,j}$ and the pitch rate q_j of the jth aircraft with

$$\alpha_{tail,j} = \alpha_{ref,j} - \frac{w_{ind,j}}{V_j} - \frac{x_{tail,j}}{V_j} q_j, \tag{26}$$

where $x_{tail,j}$ is the distance between the centre of gravity and the neutral point of the horizontal stabilizer related to the jth aircraft. The side slip angle of the stabilizer $\beta_{tail,j}$ is influenced by the roll rate p_j with

$$\beta_{tail,j} = \beta_{ref,j} - \frac{z_{tail,j}}{V_j} p_j, \tag{27}$$

where $z_{tail,j}$ is the distance between the centre of gravity and the neutral point of the ith vertical stabilizer. All other parameters are known for the reference aircraft. Combined with equation 23, the forces and moments that are generated by the aerodynamics, are known for every single aircraft and thus for the equations of motion (cf. equations 4 and 1).

3 STEADY FLIGHT MECHANIC INVESTIGATION

This section describes the steady flight mechanic investigation. Trim results as well as the power curves are presented from which enhancements for the design of the reference aircraft can be deviated.

3.1 Trim calculation

The aircraft is trimmed for a given flight condition with aerodynamic surface deflections and thrust (input values). Those values are varied by using an optimization method until an equilibrium regarding to the derivatives of the generalized speeds $\dot{u}_1, \ldots, \dot{u}_p$. The optimization is carried out with the MATLAB function `lsqnonlin` that minimizes the norm

$$\min_{\underline{x}} \|f(\underline{x})\|_2^2 = \min_{\underline{x}} \left(\sum_{j=1}^{p} \left(\dot{u}_j(\underline{x}) \right)^2 \right), \tag{28}$$

where $\underline{x}$ is the vector of the input values and f is the value for minimization. To assure physically meaningful results, a vector of lower and upper bounds for the input values is defined.

In both configurations *Conf1DJ* and *Conf2DJ*, every single aircraft can possess an individual angle of attack due to the additional pitch degree of freedom. Different possible angles of attack in the aircraft lead to a discontinuous lift distribution and consequently to a higher induced drag. For this reason, the angles of attack of all aircraft are restricted to be equal for the optimization. Due to the additional roll degree of freedom in *Conf2DJ*, every single aircraft can exhibit a different bank angle. In the case of bank angles unequal zero, a side force occurs and a higher lift is necessary to compensate the weight. This results in a higher induced drag. In order to avoid the latter, a zero bank angle of all aircraft in the formation is set as boundary condition for configuration *Conf2DJ*. Naturally, without the use of flaps, the bank angle of the outer aircraft of the formation is unequal zero because of lift distribution. At the outer parts of the wings, the lift is lower than at the inner parts. Thus a roll moment appears which will not be compensated by the joint in configuration two. Therefore, to reach an equal bank angle of all aircraft, that is zero in the considered trim condition, an additional roll moment is required. This is achieved by using the outer flaps in addition to the thrust, angle of attack and elevator deflection of the individual aircraft, as additional trim surfaces in *Conf2DJ*.

Table 1: Trim results for a single aircraft in 50 m altitude with an aispeed of 15 $\frac{\text{m}}{\text{s}}$

Thrust	F	=	2.62 N	Elevator deflection	η	=	-0.05°
Angle of attack	α	=	1.58°	Glide ratio	E	=	29.43
Induced Drag	D_{ind}	=	1.30 N	Zero Drag	D_0	=	1.19 N
Lift of wing	L_W	=	80.15 N	Lift of tail	L_T	=	-3.12 N

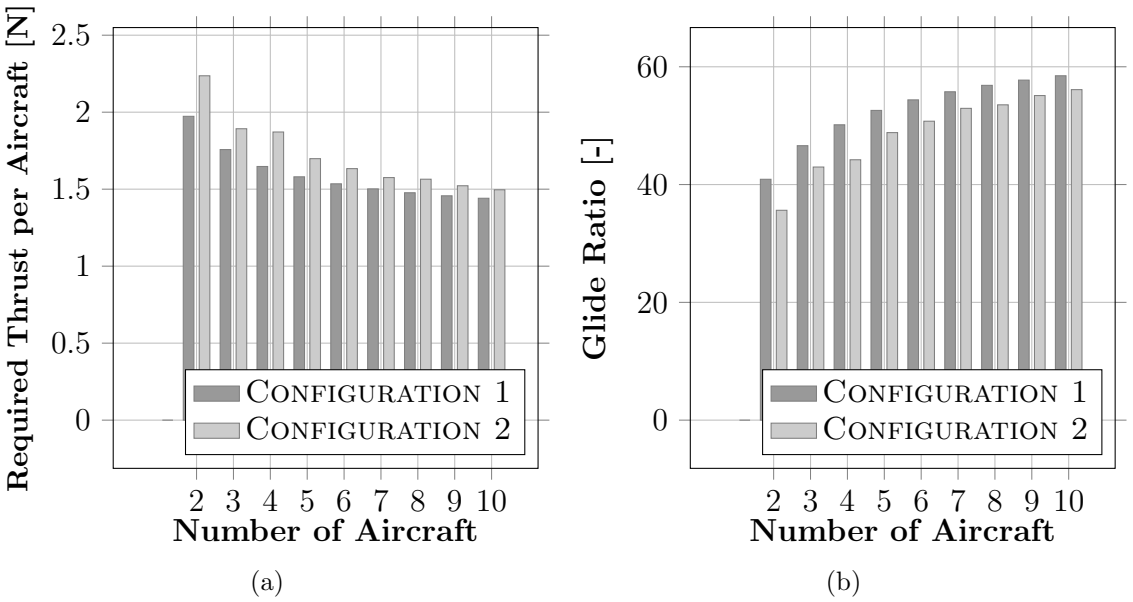

Figure 5: Trim results for the multi-body aircraft in 50 m altitude with an airspeed of 15 $\frac{\text{m}}{\text{s}}$: (a) shows the required thrust; (b) shows the glide ratio.

3.2 Trim results

In order to evaluate the multi-body aircraft in both configurations, the obtained results have to be compared to those of a single aircraft. An altitude of 50 m and an airspeed of 15 $\frac{\text{m}}{\text{s}}$, that corresponds to the minimum drag airspeed, is considered as flight conditions for all trim calculation. The trim results for a single aircraft are listed in Table 1.

In figure 5, results of the trim calculation for both configurations are illustrated. It should be noted that the zero drag for the considered configuration is calculated by the product of the zero drag from table 3.2 and the number of aircraft. It can be seen that the required thrust per aircraft for trimmed condition decreases with the number of aircraft in both configurations. For the configuration *Conf1DJ*, a reduction of a 45 % in the required thrust per aircraft in a ten coupled aircraft compared to a single aircraft is noticed. In the case of configuration *Conf2DJ*, the benefit is 43 % (cf. figure 5(a)). This difference can be explained by a higher drag due to the use of the outer wing flaps in configuration *Conf2DJ* to avoid a roll motion. In figure 6, lift's distribution of configuration *Conf2DJ* is negatively affected because of the use of flaps. However, without flaps, an equilibrium in *Conf2DJ* is not achievable.

By considering the bending moments for both configurations in figure 8, disadvantages of the first configuration become obvious. For the interpretation of the results, the lift and weight distribution, shear force as well as the bending moment for a single aircraft

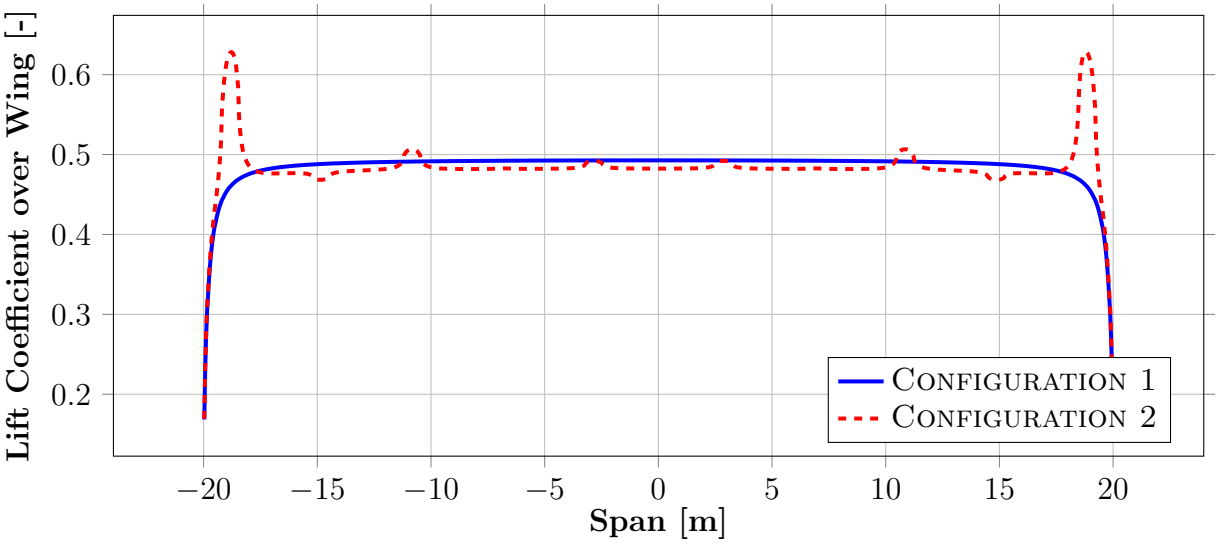

Figure 6: Exemplary illustration of lift distribution in trimmed condition for both configurations of a ten coupled aircraft.

are illustrated in figure 7. Due to the unequal distribution of weight and lift a shear force and thus a bending moment occurs. It can been seen that the mass is concentrated in the fuselage. This leads to two discontinuities in the sear force at the beginning and end of the fuselage with a sign change of the gradient. Due to the nearly linear shape of the shear force and the discontinuities, the bending moment follows a parabolic profile with a maximum in the middle of the aircraft. For the formation of ten coupled aircraft, the maximum value of the bending moment over the wing in configuration *Conf1DJ* is significantly higher than in configuration *Conf2DJ*. This can be explained by the fact that in configuration one the bending moments are transferred due to the joint (cf. figure 3). Since the distribution of weight and mass vary in the formation, the inner aircraft sustains the outer aircraft and thus a shape like the catenary occurs. In addition, the local position of this maximum bending moment in configuration *Conf1DJ* is located in the joints which are the structural weak spots of the formation. As a consequence, the structure of configuration one must be stiffer, which results in a higher structural weight, and loads at the joints appear to be higher. In contrast to *Conf1DJ*, configuration *Conf2DJ* features an equally-distributed bending moment due to joint and the impossible transmission of bending moments. This has the advantage that all separate aircraft can be designed structurally identical. Thus, an arbitrary coupling of the aircraft is possible. Because of the fact that the disadvantages outweigh the advantages in the first configuration, the second configuration is selected for the multi-body aircraft.

3.3 Modification in aircraft design

Considering the lift distribution over the wing in figure 6, two problems arise. The main difference between both configurations is the use of flaps for trimming in configuration *Conf2DJ*. The flaps' deflection leads to a higher drag. Beside the influence on the drag, another effect has has to be taken into account. In *Conf2DJ* the wing tip exhibits a high lift coefficient. This also results from the flaps' deflection. A high lift coefficient amplifies the stall hazard, especially in turning flight when the airspeed decreases at the inner wing. In order to avoid these negative effects, the roll moment has to be compensated without aerodynamic forces. A suitable approach seems to be a lateral variation of the centre of

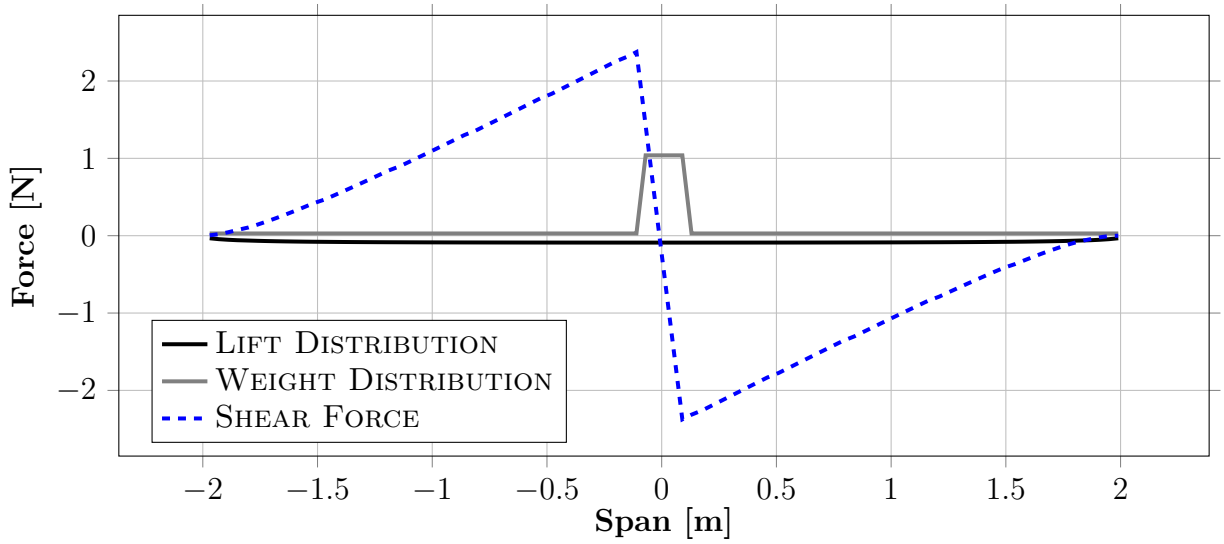

(a) Structural forces

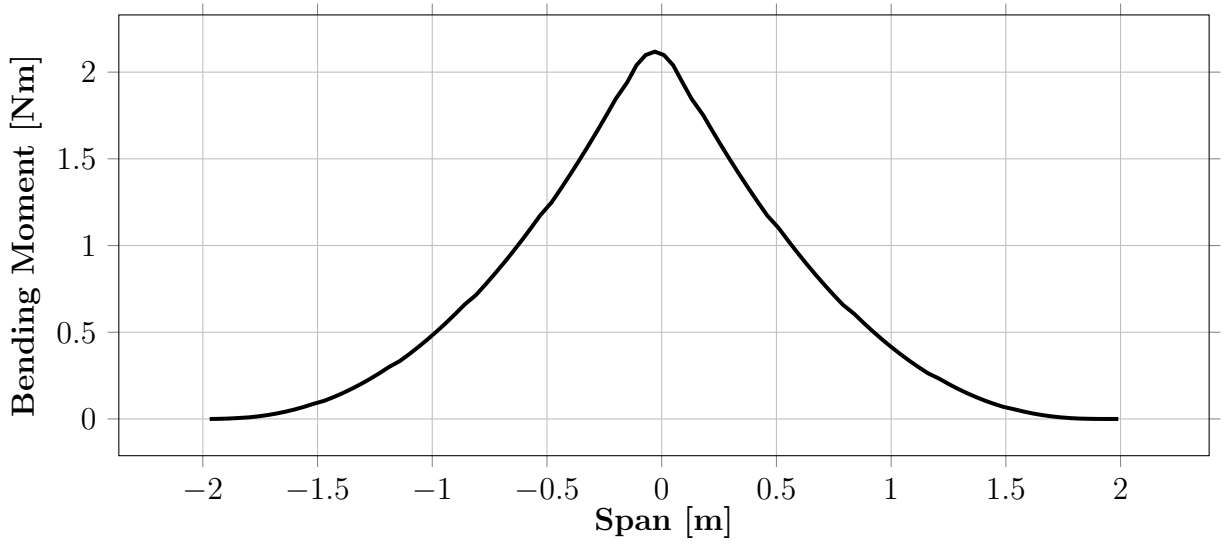

(b) Bending moment

Figure 7: Illustration of structural force and moment for a single aircraft

gravity that leads to a different mass distribution. As a result of this change, the lever arms of the aerodynamic forces are affected and thus the roll moment. This principle is well known from conventional airliners to trim the pitch moment with fuel balancing. However, as the multi-body aircraft will be operated electrically, an alternative has to be found. With the help of a rail system with a mass, which can be the accumulator's one, can be placed left or right from the origin centre of gravity so that the roll moment that might appear is compensated. The new position in y direction of the centre of gravity is calculated with

$$y_{\text{CG, new}} = y_{\text{CG,old}} + y_{\text{displacement}} \frac{m_{\text{displacement}}}{m_{\text{total}}}, \tag{29}$$

where $y_{\text{displacement}}$ is the displacement of the trim mass $m_{\text{displacement}}$ [18]. Beside the centre of gravity, the moment of inertia around the x axis is influenced by a displacement of a trim mass. Therefore, the Huygens-Steiner theorem (parallel axis theorem) [18] has to be

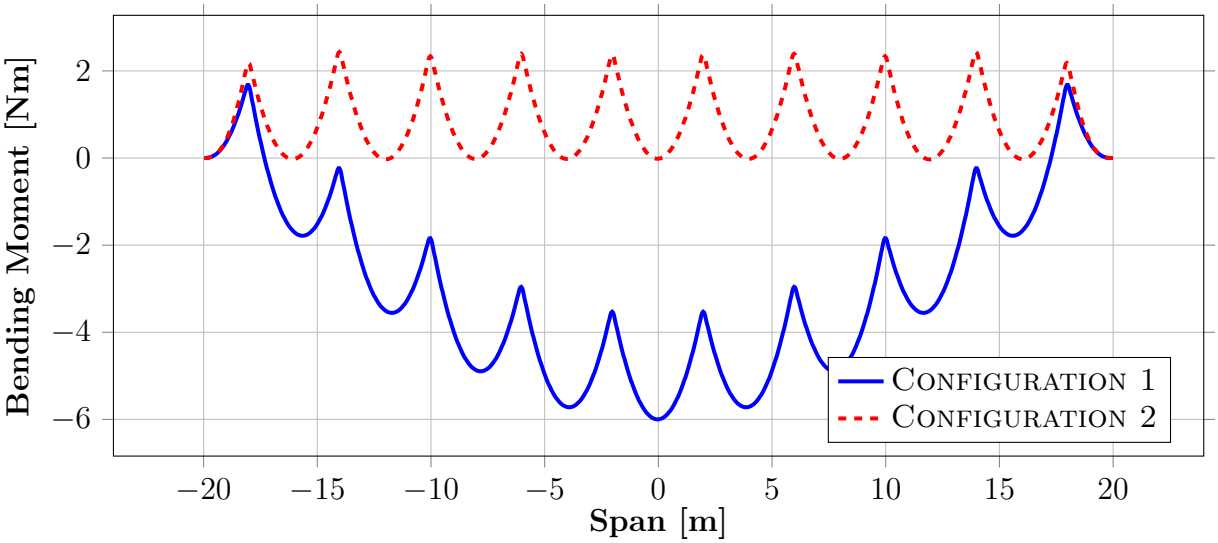

Figure 8: Bending moment in trimmed condition for both configurations of a ten coupled aircraft.

applied to the moment of inertia. This leads to

$$J_{xx,\,\text{new}} = J_{xx,\,\text{old}} + m_{\text{total}}\left(y_{\text{CG},\,\text{new}} - y_{\text{CG,old}}\right)^2 \tag{30}$$

as new moment of inertia due to a displacement of the trim mass in y direction.

Table 2: Required shift of the centre of gravity in y direction to achieve a steady state for second configuration depending on the number of coupled aircraft

Number of aircraft	Shift of the centre of gravity in y-direction [m]									
	1	2	3	4	5	6	7	8	9	10
2	0.1	-0.1								
3	0.16	0.00	-0.16							
4	0.19	0.09	-0.09	-0.19						
5	0.22	0.14	0.00	-0.14	-0.22					
6	0.23	0.18	0.06	-0.06	-0.18	-0.23				
7	0.24	0.22	0.11	0.00	-0.11	-0.22	-0.24			
8	0.25	0.24	0.15	0.05	-0.05	-0.15	-0.24	-0.25		
9	0.26	0.26	0.18	0.09	0.00	-0.09	-0.18	-0.26	-0.26	
10	0.27	0.27	0.21	0.13	0.04	-0.04	-0.13	-0.21	-0.27	-0.27

The required shift of the centre of gravity for trimmed conditions was calculated. The results are presented in table 2. Considering the available width of the fuselage of the generic UAV, it seems to be impossible to shift for example the accumulator inside the fuselage to reach a steady state. Furthermore, table 2 presents the shift in centre of gravity and not the required distance of moving a trim mass. For the required position of the trim mass, the results of table 2 have to be multiplied with the quotient of the total mass of the aircraft and the trim mass (cf. equation 29). Considering a multi-body aircraft with ten coupled aircraft and the accumulator as trim mass (m = 1 kg), a shift of 2.22 m is required. This is more than the half span length of the aircraft. For the successful use of the method, the trim mass has to increase and the shifting system has to be integrated

in the wing or in another conduit. This affects either the maximal payload or the zero drag of the aircraft. Nevertheless, a lift distribution equal to the first configuration as illustrated in figure 6 is achieved, while the benefits in regard to the required thrust are preserved. Therefore, the presented method for trimming the aircraft shall be used in the following investigations without considering the disadvantages of the method. For designing a multi-body HALE aircraft this problem has to be taken into account and solved.

3.4 Power Curve

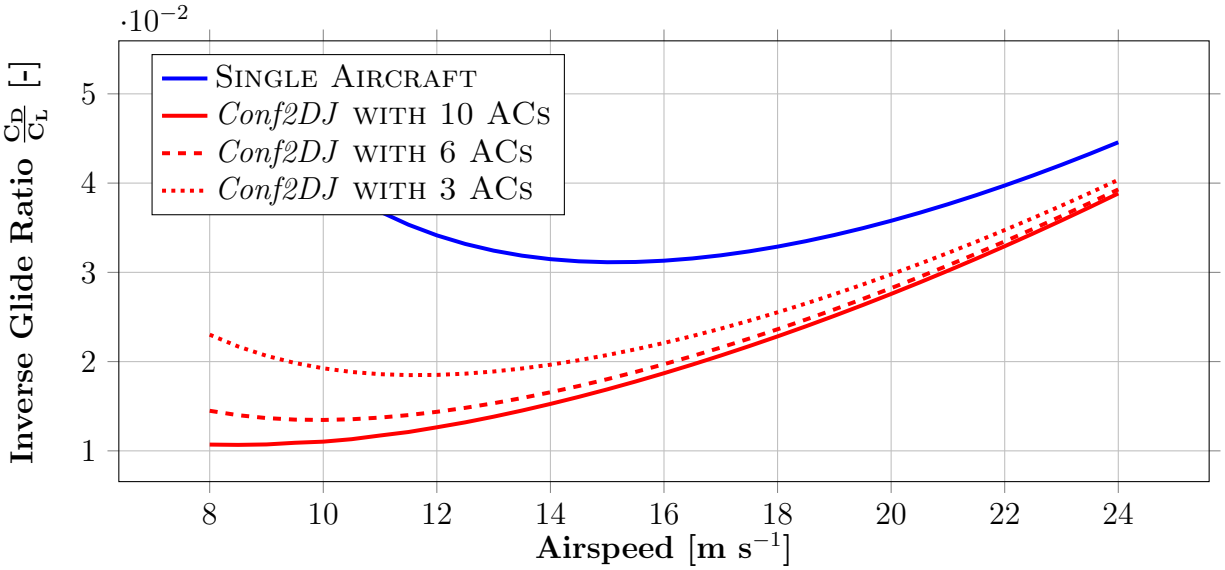

Figure 9: Power Curve for a single aircraft and a multi-body aircraft in configuration two with ten aircraft.

In flight performance investigation, the power curve can be used to determine the minimum drag airspeed and the best glide ratio. For a single aircraft and a multi-body aircraft with three, six and ten single aircraft in configuration *Conf2DJ*, the inverse glide ratio depending on the airspeed is illustrated in figure 9. It is obvious that the inverse glide ratio over the airspeed for the multi-body aircraft are distinctly lower than for the single aircraft. By an increasing number of coupled aircraft, the aspect ratio is increased and thus the induced drag. This leads to lower minimum drag speeds for a higher number of coupled aircraft. Apart from the advantages of a lower induced drag, the lift coefficient is increased at lower airspeed. Currently, there is no stall model implemented in the aerodynamic model. Nevertheless, regarding to [7], it is assumed that the maximal lift coefficient is 1.5. This maximum value must be avoided in steady flight, because a margin in case of gust, turbulence or maneuver is required. For ten coupled aircraft, the required lift coefficient for the minimum drag airspeed at 8.5 $\frac{\text{m}}{\text{s}}$ is 1.52. This lift coefficient is impossible in practical terms. Considering a higher airspeed, like 14 m/s, the glide ratio decreases significantly and the lift coefficient is 0.62. Thus, the latter is far beneath the maximum lift coefficient allowed. In this flight condition, the required power per aircraft amounts to 19 W in comparison to 39.28 W for the single aircraft at 15 $\frac{\text{m}}{\text{s}}$. This results in a power saving of approximately 50 %. Considering the minimum drag speed for a formation of six coupled aircraft, a lift coefficient of 1.2 and a required power per aircraft of 15.5 W is achieved. However, the payload is reduced. In the case of the minimum drag speed for three coupled aircraft, the formation possesses a lift coefficient of 0.9 with a required

power per aircraft of 20.81 W. Thus it is evident that there is an optimum relating to efficiency in considering the permitted lift coefficient and the pay load. In addition to the shift of the centre of gravity, this optimum has to be evaluated in the final design of the multi-body aircraft with the purpose as HALE aircraft.

Considering the gradient of the power curves, it can be noticed that the higher the velocity in relation to the minimum drag airspeed, the lower the aerodynamic efficiency. For multi-body aircraft the gradient is higher than for single aircraft. As a consequence, the multi-body aircraft has to be operated close to the airspeed of minimum drag. Otherwise the benefits of the configuration for a lean use of energy cannot be used.

4 DYNAMIC FLIGHT MECHANIC INVESTIGATION

After having performed the steady flight mechanic analysis of the multi-body aircraft, the dynamic investigation can be carried out. The dynamic behavior is investigated with the linear state space description around the steady state and thus with the eigenvalues of the aircraft. Furthermore, studies in time domain with the full nonlinear equations and the linearized state space system are carried out with the help of a numerical simulation. The results are compared to each other in order to validate the influence of nonlinearities. Based on the comparison, a suitable method for control law design can be derived.

4.1 Analysis of the dynamic behavior with state space models

The equations of motion for a single aircraft are nonlinear. Those nonlinearities result from the kinematics (e.g. Euler angle) and the forces. Due to the coupling of several aircraft, the level of nonlinearities is increased. For a linear investigation, the nonlinear equations of motion have to be linearized. For this purpose, a Simulink model is created. It includes models for all external forces, the kinematic and time integration. In the process of integration, only the generalized speeds and the Euler angles are used. In the context of dynamic flight mechanic investigation, the equations position and azimuth angle are not needed. This diminishes the number of differential equations (and integrations) from twelve to eight for the single aircraft. Relating to [2] and [11], the state vector

$$\underline{x} = \left[\underbrace{q, \quad \alpha, \quad V, \quad \gamma}_{\text{Longitudinal motion}}, \quad \underbrace{r, \quad \beta, \quad p, \quad \Phi}_{\text{Lateral motion}} \right]^T \tag{31}$$

is used for an unique description of the single aircraft. As aircraft are coupled, the number of state variables increases depending on the coupling configuration. In configuration *Conf1DJ*, another aircraft leads to an additional pitch motion between the aircraft. Thus, the state vector is extended to include the pitch rate and the pitch angle of the additional aircraft. For n aircraft in configuration one, the number of states is given by

$$\text{No. of States} = 8 + 2\ (n-1). \tag{32}$$

In configuration *Conf2DJ* an additional roll motion between the aircraft is possible. This results in an enlargement of the state vector to the roll rate and the roll angle. In the case of n aircraft, the number of states is computed with

$$\text{No. of States} = 8 + 4\ (n-1). \tag{33}$$

To determine the state space representation of the multi-body aircraft regarding to the number of aircraft and the state vector, the Simulink model is linearized around the steady horizonal flight (see chapter 3.2) using Matlab. This yields the linear state space differential equation

$$\dot{\underline{x}} = \underline{\underline{A}}\ \underline{x} + \underline{\underline{B}}\ \underline{u} + \underline{\underline{E}}\ \underline{z} \tag{34}$$

where the thrust and the control surface deflections (elevator as well as left and right rudder, flap and aileron) of all aircraft are elements of the input vector $\underline{u}$ and the wind velocity in all directions are elements of the disturbance vector $\underline{z}$. Depending on the aircraft number n, the number of input variables is 8 n and the number disturbance variables is 3 n. The eigenvalues of the dynamic matrix $\underline{\underline{A}}$ determine the dynamic behaviour of the multi-body aircraft. In a first step, the joints between all aircraft are assumed as fully rigid. This results in six degrees of freedom, independent of the number of aircraft. In this way, the effects of multiple aircraft on the rigid body modes can be evaluated. In the following subsections, the eigenvalues and eigenvectors of *Conf1DJ* and *Conf2DJ* are investigated.

4.1.1 Eigenvalues of fixed connected aircraft

Table 3: Characteristic parameter of the five basic flight dynamic modes for a fixed joint connection depending on the number of coupled aircraft

	Number of aircraft							
	1	2	3	4	5	6	7	8
Short period mode								
ω_{SP} [rad s^{-1}]	19.3	19.8	19.9	20.0	20.01	20.02	20.02	20.02
D_{SP} [1]	0.79	0.78	0.77	0.77	0.77	0.77	0.77	0.77
Phugoid mode								
ω_{PH} [rad s^{-1}]	0.74	0.73	0.73	0.73	0.73	0.73	0.73	0.73
D_{PH} [1]	0.02	0.02	0.03	0.03	0.03	0.03	0.03	0.03
Dutch roll								
ω_{DR} [rad s^{-1}]	5.84	2.02	1.31	1.00	0.83	0.72	0.64	0.59
D_{DR} [1]	0.08	0.25	0.38	0.49	0.6	0.68	0.76	0.83
Roll mode								
T_{R} [s]	0.11	0.11	0.11	0.11	0.11	0.11	0.11	0.11
Spiral mode								
$T_{2,\mathrm{SM}}$ [s]	1.63	5.55	9.53	12.18	14.06	15.65	17.33	19.04

A rigid body aircraft has five flight dynamic modes: The short-period and the phugoid modes in longitudinal motion. The dutch roll, spiral and roll modes in the lateral motion. The characteristic parameters of the five flight dynamic modes for a fix joint connection for one up to eight coupled aircraft are presented in table 3. The damping ratio and natural frequency of the short period and the phugoid mode are not influenced by an increasing number of coupled aircraft. The time constant of the roll mode is not altered by an increasing number of aircraft. This can be justified by the fact that the span's length and moment of inertia increase with the number of joined aircraft. The influence on the

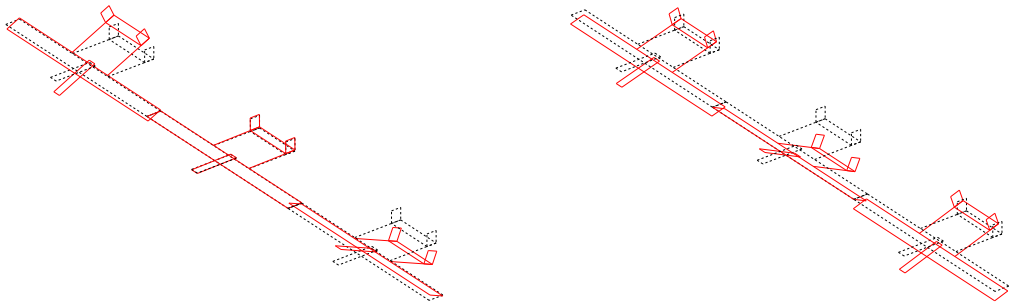

(a) $\lambda_{1,2} = -17.4 \pm i\ 9.94$, $D = 0.87$, $\omega = 20.01\ \frac{\text{rad}}{\text{s}}$ (b) $\lambda_{3,4} = -6.08 \pm i\ 2.34$, $D = 0,93$, $\omega = 6.52\ \frac{\text{rad}}{\text{s}}$

Figure 10: Illustration of the eigenmodes and characteristic parameters relating to the addional pitch oscillations while using three coupled aircraft in configuration *Conf1DJ* according to the pitch rate

Dutch roll and the spiral mode is quite significant. The damping ratio raises with a higher number of coupled aircraft, whereas the frequency of the Dutch mode decreases. Both variations can be justified with the increase of span's length due to the yawing motion is influenced and the additional number of vertical stabilizers. Finally, the spiral mode is an unstable motion independent of the number of aircraft, but the time to double increases with a higher number of coupled aircraft. This leads to a more controllable spiral mode, if the number of aircraft is increased.

4.1.2 Eigenvalues of Conf1DJ

Table 4: Characteristic parameter of the five basic flight dynamic modes for configuration one depending on the number of coupled aircraft

	Number of aircraft								
	2	3	4	5	6	7	8	9	10
Short period mode									
ω_{SP} [rad s^{-1}]	19.8	20.0	20.01	20.01	20.02	20.02	20.02	20.02	20.03
D_{SP} [1]	0.78	0.78	0.77	0.77	0.77	0.77	0.77	0.77	0.77
Phugoid mode									
ω_{PH} [rad s^{-1}]	0.73	0.73	0.73	0.73	0.73	0.73	0.73	0.73	0.73
D_{PH} [1]	0.02	0.02	0.02	0.02	0.02	0.02	0.02	0.02	0.02
Dutch roll									
ω_{DR} [rad s^{-1}]	2.13	1.39	0.94	1.08	0.84	0.75	0.67	0.64	0.60
D_{DR} [1]	0.14	0.06	0.07	0.06	0.08	0.07	0.11	0.08	0.10
Roll mode									
T_{R} [s]	1.01	1.15	1.02	1.05	1.05	1.07	1.08	1.11	1.12
Spiral mode									
$T_{2,\text{SM}}$ [s]	1.03	3.54	2.43	2.88	2.75	3.17	3.00	3.71	3.85

Beside the rigid body modes, in configuration *Conf1DJ*, depending on the number of

coupled aircraft n, $n-1$ additional pitch oscillations occur. One of these oscillations possesses a frequency close to the the short-period mode's one, but its damping is higher. The other $n-2$ pitch oscillations have a frequency close to $\omega = 6,52\ \frac{\text{rad}}{\text{s}}$ and a damping around $D = 0,93$. Due to the high damping of the additional pitch oscillation with the lower frequency, beginning with a formation of five coupled aircraft the oscillation changes to two aperiodic motions. The eigenforms of both additional pitch oscillations are shown in figure 10. The first pitch oscillation represents a antisymmetric pitch motion of the two outer aircraft. The second oscillation contains a symmetric pitch rate between the two outer aircraft. For all number of coupled aircraft, the flight mechanic modes are clearly identified. The characteristic parameters for the basic flight dynamic modes are presented in table 4. In comparison to the results of table 3, differences in the lateral motion are evident. The time to double of the spiral does not increase any longer significantly with the number of couples aircraft. The damping of the Dutch roll is no longer increased with more coupled aircraft. For all number of coupled aircraft in *Conf1DJ*, the Dutch roll is a low damped oscillation. This can be explained by the fact that the yaw motion influences the airspeed of the different coupled aircraft. This change of speed affects the aerodynamic forces and moments and thus a pitch motion occurs. As a result the angle of attack and the lift distribution of the whole formation is influenced. Due to the influence of the yaw rate to the pitch motion of every aircraft, the longitudinal states could not be neglected in lateral modes.

4.1.3 Eigenvalues of Conf2DJ

Table 5: Number and Type of eigenvalues for a multi-body aircraft in configuration two depending on the number of coupled aircraft

	Number of coupled aircraft								
	2	3	4	5	6	7	8	9	10
Stable Modes									
Complex Eigenvalues	4	5	6	9	10	11	12	14	14
Real Eigenvalues	2	2	3	2	3	4	4	3	5
Unstable Modes									
Complex Eigenvalues	0	1	2	1	1	1	2	4	4
Real Eigenvalues	2	2	1	2	3	4	2	1	3
Number of Modes	8	9	14	17	23	20	20	22	26
Sum of Eigenvalues	12	16	20	24	28	32	36	40	44

The dynamic matrices in trimmed conditions for configuration two present a distinct number of modes compared to the previous investigations. The number and type of eigenvalues for all possible aircraft formations are presented in table 5. A more detailed investigation of all possible formations in this configuration is beyond the scope of this paper.

The interdepedance of the lateral basic flight modes and the states that occur due to the additional degrees of freedom is much more significant in this configuration than in configuration *Conf1DJ*. An unambiguous identification of the Dutch roll, spiral and roll mode with the help of the eigenvectors is not feasible for most of the considered

Table 6: Characteristic parameter of the longitudinal flight dynamic modes for configuration two depending on the number of coupled aircraft

	Number of aircraft								
	2	3	4	5	6	7	8	9	10
Short period mode									
ω_{SP} [rad s^{-1}]	19.80	19.30	19.40	19.70	20.10	20.02	20.01	20.02	20.01
D_{SP} [1]	0.77	0.76	0.78	0.78	0.78	0.77	0.77	0.77	0.77
Phugoid mode									
ω_{PH} [rad s^{-1}]	0.73	0.82	0.77	0.76	0.73	0.70	0.61	0.69	0.72
D_{PH} [1]	0.02	-0.05	-0.08	0.03	0.04	0.07	0.10	-0.01	-0.01

formations. The influence from the lateral states to the additional states and thus to the longitudinal states is excessive. As a consequence the parameters of the lateral flight mechanic modes are not presented for this configuration. Even the application of the modal assurance criterion (MAC) [3] for the identification of the lateral modes does not enable an unambiguous assignment. However, with the comparison of the characteristic parameter to the previous results and the analysis of the eigenvector, an identification of the longitudinal modes is feasible. The results are presented in table 6. It should be noted that the additional degrees of freedom relating to the roll motion also influence the phugoid mode. The vertical motion in this mode affects the local angle of attack and thus a roll motion occurs. In some configurations this effect leads to an unstable phugoid that is well-known from highly flexible aircraft [1].

In order to illstrate the occurring modes, a formation of three couples aircraft will be analyzed in detail. The ten eigenmodes and associated parameters are presented in figure 11 for a formation of three coupled aircraft in configuration *Conf2DJ*. The first mode is an aperiodic yaw motion that is similar to the spiral mode. The evaluation of the MAC offers a conjugal agreement. From the illustration, it becomes obvious that the aircraft motions are not in phase. The pitch and roll motion of the separate aircraft are involved in this mode. The second mode is an unstable oscillation. Regarding to the eigenvector and the frequency, this mode is similar to the phugoid mode. As postulated before, the roll motion of the outer aircraft is involved in this mode. The MAC regarding to the third mode shows a strong correlation to the Dutch roll. The yaw rate is participating in this mode. However, the bank angles of the single aircraft are not in phase. This results from the coupling of yaw motion and velocity that leads to an influence on the lift disturbance. The next illustrated mode is an unstable aperiod mode in which the bank angle of two aircraft is identical, but the third aircraft possesses a bank angle with a different sign. It is comparable to two adverse roll motions of two components of the formation. The fifth mode is a stable roll oscillation of the outer aircraft. This mode occurs due to the joint and the additional roll degree of freedom between the aircraft. The sixth mode offers an unstable aperiodic motion with a low time to double. The outer wing increase symmetrically the bank angle and this results in a decrease of the lift. Using the MAC, the next mode is similar to the roll mode. Because of the scaling of the values of the eigenvector, only the opposed pitch motion of the outer aircraft which is a result of the roll motion can be seen and not the roll motion itself. The last three modes are pitch oscillations which

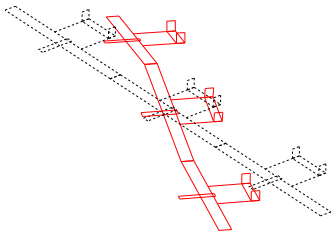

(a) $\lambda_1 = 0.147$, $T_2 = 4.715$ s

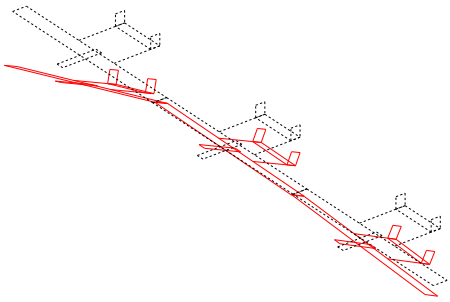

(b) $\lambda_{2,3} = 0.041 \pm i\ 0.82$, $D = -0.05$, $\omega = 0.82\ \frac{\text{rad}}{\text{s}}$

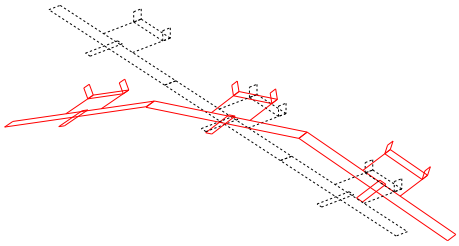

(c) $\lambda_{4,5} = -0.4 \pm i\ 1.0$, $D = 0.37$, $\omega = 1.08\ \frac{\text{rad}}{\text{s}}$

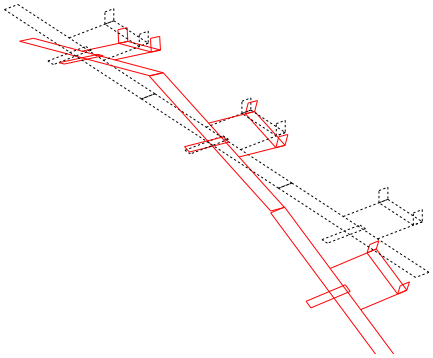

(d) $\lambda_6 = 1.4$, $T_2 = 0.5$ s

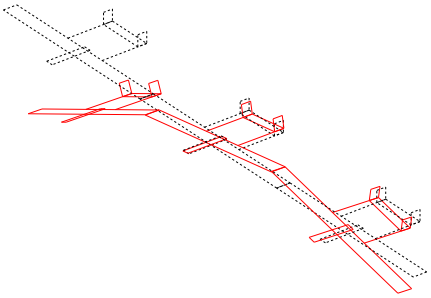

(e) $\lambda_{7,8} = -0.231 \pm i\ 1.72$, $D = 0.13$, $\omega = 1.73\ \frac{\text{rad}}{\text{s}}$

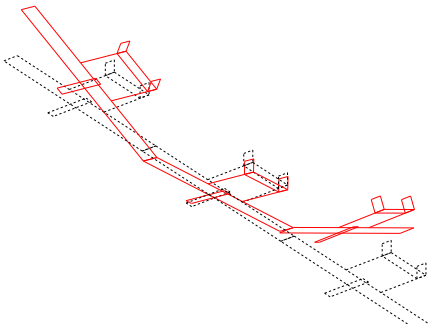

(f) $\lambda_9 = -2.63$, $T_1 = 0.38$ s

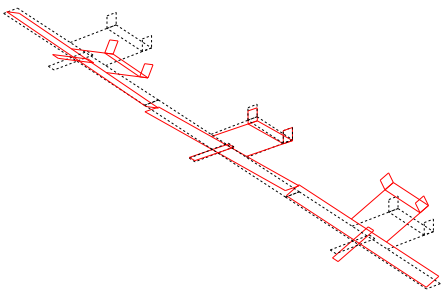

(g) $\lambda_{10} = -1.72$, $T_1 = 0.58$ s

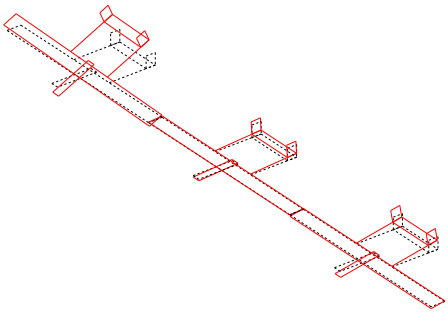

(h) $\lambda_{11,12} = -12.8 \pm i\ 11.0$, $D = 0.76$, $\omega = 1.68\ \frac{\text{rad}}{\text{s}}$

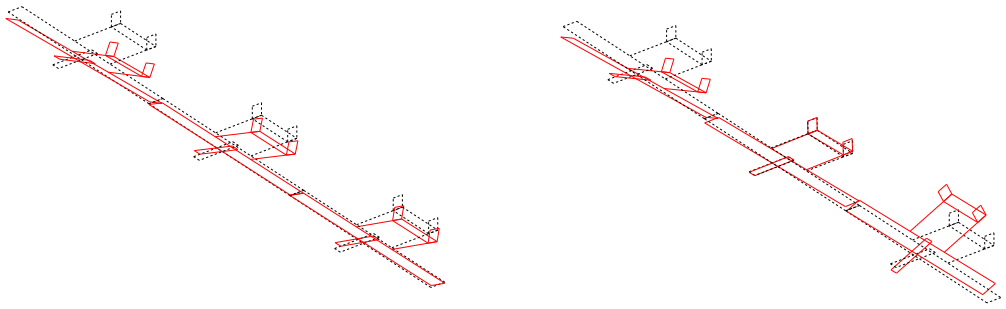

(i) $\lambda_{13,14} = -14.7 \pm i\ 12.5$, $D = 0.76$, $\omega = 19.3\ \frac{\text{rad}}{\text{s}}$ (j) $\lambda_{15,16} = -19.4 \pm i\ 13.1$, $D = 0.83$, $\omega = 23.4\ \frac{\text{rad}}{\text{s}}$

Figure 11: Illustration of the eigenmodes with regard to the rotation rates for a multi-body aircraft with three coupled aircraft in configuration *Conf2DJ*

are similar to *Conf1DJ*. Due to the same phase of the pitch rate in the ninth mode, this mode is identified as short period mode.

4.2 Results of numerical simulation

The investigation of the influence of the nonlinearities to the dynamic behavior of the formation is carried out with a numerical simulation of the linear and nonlinear model. In a formation with four coupled aircraft in the second configuration, the elevators of both inner aircraft are deflected to minus one degree after one second. The response regarding to the pitch rates for the linear and the fully nonlinear model for the short time dynamic is illustrated in figure 12. In all pitch responses the short period mode can be seen. The results for the linear and the nonlinear model are consistent for this eigenmode. After the short period mode is dying out, the response for the linear and nonlinear model diverge from each other. This leads to the fact that the nonlinearities have a strong impact on the dynamic behavior. This effect is well known for highly flexible aircraft [14]. Thus the joint permits a highly flexible roll and pitch motion. The high effect of the nonlinearities to the dynamic behavior for a multi-body aircraft was expected.

With this short investigation, a complete analysis of the dynamic behavior in the time domain is not yet completed. The reaction force, the lateral motion and the behavior of the other states have to be taken into account. This short investigation should only be used for the evaluation of the nonlinear influence.

4.3 Requirements for flight control system

The previous investigation relating to the dynamic behavior enables first conclusions for the required flight control system as well as for the design of the controller. The analyzed eigenvalues for configuration *Conf2DJ* exhibit some unstable harmonic and aperiodic eigenmodes. Those unstable motions must be stabilized in any case of trimmed conditions in order to avoid fatal consequences. In classical flight control law design, inner loops, which are for example designed with pole placements or eigenstructure assignment, are used for the stabilization and improvement of handling qualities [16]. This is an appropriate approach, if the plant is robust enough. The results of the numerical simulation show a divergence between the linear state space model and the nonlinear model after

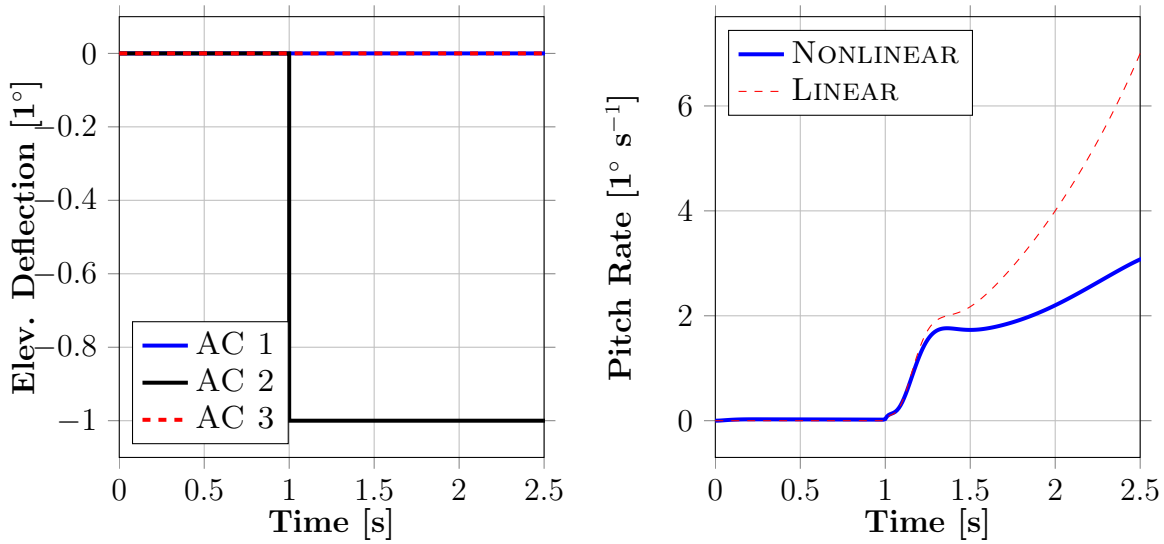

(a) Elevator Deflection

(b) Pitch Rate Aircraft 1

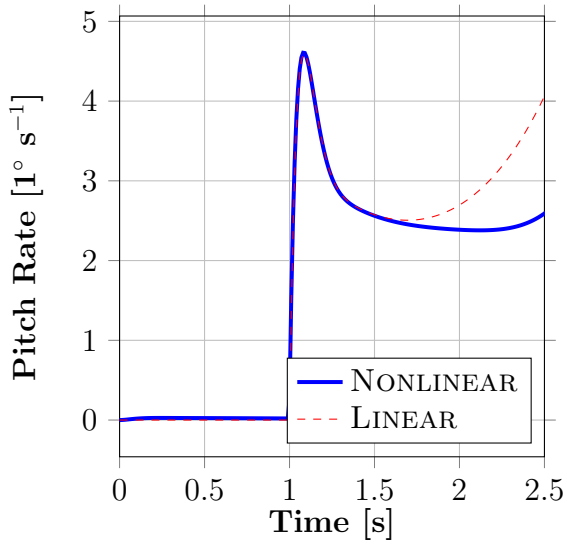

(c) Pitch Rate Aircraft 2

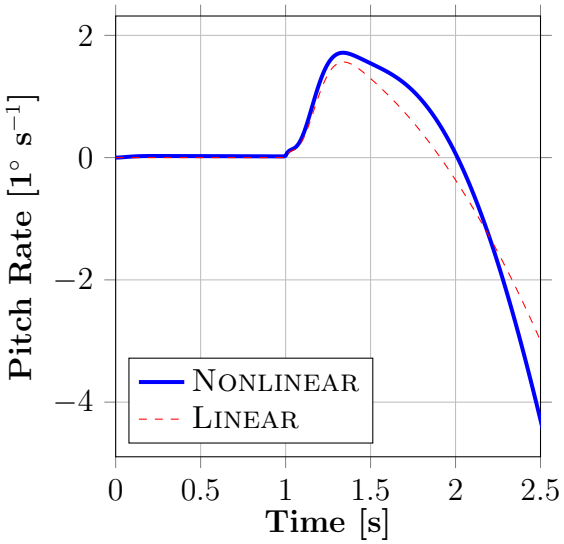

(d) Pitch Rate Aircraft 3

Figure 12: Illustration of the step response for an elevator deflection in a formation with three coupled aircraft in configuration *Conf2DJ* regarding to the pitch rate

a short time. This fact allows the conclusion that linear methods are not applicable to stabilize the formation. Nonlinear methods have to be used. Another approach is the use of a robust control law design. This method fits well for nonlinear systems by summing up the nonlinearities in uncertainties and design the control regarding to robust stability and robust performance [15]. Furthermore, lateral and longitudinal motion are considered as independent in classical flight control design [16]. This is justified with the assumption that the state of lateral and longitudinal motions have no impact on each other. This is not the case for the multi-body aircraft. Hence a flight control law design has to take both motions into account.

In addition to the stabilization, the control system shall ensure that the reaction forces are small enough and a satisfactorily aerodynamic state is achieved which results in excellent flight performance. Especially the reaction forces are not yet considered in the time

domain investigation. If those requirements are fulfilled, a control system for the guidance can be set up.

5 CONCLUSION AND OUTLOOK

This paper introduced a new aircraft concept. A theoretical basis has been presented for modeling and analyzing a multi-body aircraft. Two configurations of coupling the aircraft have been taken into account. Because of an individual angle of attack of every single aircraft, the (unsymmetrical) effect of gust loads can be reduced. This is a huge advantage compared to highly flexible aircraft. The equations of motion that are highly nonlinear were assembled by using Kane's method. Contrary to the structural geometrical nonlinearities of highly flexible aircraft, those nonlinearities are described mathematically exact. Trim results were presented for both configurations and a high amount of benefit regarding to the required power was observed. This allows a long operation time and is thus satisfying one requirement for a HALE aircraft. However, it is important to ensure that the lift coefficent is low enough to avoid stall due to aerodynamic loads. This leads to an optimization problem in the aircraft design of a multi-body HALE aircraft. Configuration *Conf2DJ* possesses a low bending moment which allows the use of light materials. The disadvantage of a local high lift coefficient at the outer wings due to the use of flaps for trimmed conditions was solved by shifting the centre of gravity. However, the final aircraft design for the HALE-aircraft must ensure that a suitable facility for the movement of a trim mass is available. Besides the steady flight mechanical investigation, a dynamic analyze of the multi-body aircraft was carried out. The influence of the coupling effects to the basic flight mechanic modes was shown. It turned out that there are unstable modes for *Conf2DJ*. Furthermore, it was presented that the plant contains a highly nonlinear behavior and that lateral motion and longitudinal motion have an influence on each other. This effect must be taken into account for flight control law design. Based on the result of for the steady flight mechanic investigation for a generic UAV, the multi-body aircraft seems to be a suitable alternative to highly flexible aircraft for operating in high altitudes for long endurance. Regarding the design of a single aircraft that is usable to form a HALE-aircraft, an optimization must be carried out, to reach an optimum in structural and aerodynamic aspects.

Based on this investigation, a preliminary aircraft design for a multi-body aircraft that operates as a HALE-aircraft is feasible and will be carried out. The effect that occurs from the coupling are now known and will be taken into account in the design process. For a more detailed representation of the external forces, the aerodynamic model should be extended to unsteady aerodynamic effects. Requirements for the flight control law should be defined and a suitable approach used for the control law design.

6 References

[1] Cesnik, Carlos E., and Senatore, Patric J., and Su, Weihua, and Atkins, Ella M., and Shearer, Christopher M., and Pitcher, Nathan A. *X-HALE: A Very Flexible UAV for Nonlinear Aeroelastic Tests*. Paper No. AIAA-2010-2715, 2010

[2] Etkin, Bernard, and Lloyd Duff Reid. *Dynamics of flight: stability and control*, Vol. 3, Wiley, 1996

[3] Fu, Zhi-Fang, and He, Jimin. *Modal Analysis*, Butterworth-Heinemann, 2001

[4] Huston, Ronald L. *Multibody dynamics*, Butterworth-Heinemann, 1990.

[5] Kane, Thomas R., and Levinson, David A. *Dynamics, theory and applications*, McGraw Hill, 1985.

[6] Katz, Joseph, and Plotkin , Allen. *Low-speed aerodynamics*, Vol. 13, Cambridge University Press, 2001

[7] Kostic, Ivan A., and Stefanovic, Zoran A., and Kostic, Olivera P. *Aerodynamic analysis of a light aircraft at different design stages*, FME Transactions 42.2 (2014): 94-105.

[8] Lee, Bohwa, and Poomin Park, and Chuntaek Kim. *Power Managements of a Hybrid Electric Propulsion System Powered by Solar Cells, Fuel Cells, and Batteries for UAVs.* in *H*andbook of Unmanned Aerial Vehicles, Springer, 2014

[9] Levinson, David A., and Kane, Thomas R. *AUTOLEV - a new approach to multibody dynamics.*, in *Multibody Systems Handbook*, Springer, 1990: 81-102.

[10] Phillips, Warren F. *Mechanics of Flight*, Wiley, 2004

[11] McRuer, Duane T., and Dunstan Graham, and Irving Ashkenas. *Aircraft dynamics and automatic control*, Princeton University Press, 2014

[12] Sadraey, Mohammad. *Aircraft Performance: Analysis*, VDM Publishing, 2009

[13] Schlichting, Hermann, and Truckenbrodt, Erich. *Aerodynamik des Flugzeuges*, Springer, 1969.

[14] Shearer, Christopher M., and Cesnik Carlos E. *Nonlinear flight dynamics of very flexible aircraft*, Journal of Aircraft 44.5 (2007): 1528-1545

[15] Skogestad, S., and Postlethwaite, I. *Multivariable Feedback Control: Analysis and Design*, Wiley, 2005

[16] Stevens, B.L., and Lewis, F.L. *Aircraft Control and Simulation*, Wiley, 2003

[17] Su, Weihua, and Cesnik, Carlos E. *Dynamic response of highly flexible flying wings*, AIAA journal 49.2 (2011): 324-339

[18] Wittenburg, Jens. *Dynamics of Systems of Rigid Bodies*, Vieweg+Teubner Verlag, 2013

COPYRIGHT STATEMENT

The authors confirm that they, and/or their company or organization, hold copyright on all of the original material included in this paper. The authors also confirm that they have obtained permission, from the copyright holder of any third party material included in this paper, to publish it as part of their paper. The authors confirm that they give permission, or have obtained permission from the copyright holder of this paper, for the publication and distribution of this paper as part of the IFASD 2015 proceedings or as individual off-prints from the proceedings.